Coastal Engineering 83 (2014) 1–14

Contents lists available at ScienceDirect

Coastal Engineering

journal homepage: www.elsevier.com/locate/coastaleng

Measurement and modelling of the influence of grain size and pressure gradient on swash uprush sediment transport

Ilya K. Othman [a,b,*], Tom E. Baldock [a], David P. Callaghan [a]

[a] School of Civil Engineering, University of Queensland, St Lucia, Brisbane, Queensland 4072, Australia
[b] Faculty of Civil Engineering, Universiti Teknologi Malaysia, Skudai, Johor 81310, Malaysia

ARTICLE INFO

Article history:
Received 27 June 2013
Received in revised form 11 September 2013
Accepted 12 September 2013
Available online 9 October 2013

Keywords:
Sediment transport
Swash
Dam break
Uprush
Grain size
Meyer-Peter Muller

ABSTRACT

The paper examines the dependency between total sediment transport, q, and grain size, D (i.e. $q \propto D^p$) under dam break generated swash flows. Experiments were performed in a dam break flume over a sloping mobile sand bed with median grain sizes ranging from 0.22 mm to 2.65 mm. The total sediment transport was measured by truncating the flume bed and collecting the sediment transported over the edge. The experiments were designed to exclude pre-generated turbulence and pre-suspended sediment so as to focus solely on the swash flow. The magnitude and nature of the grain size dependency (i.e. p value) were inferred for different flow parameters; the initial dam depth, d_o, the integrated depth averaged velocity cubed, $\int u^3 dt$, and against the predicted transport potential, q_p, using the Meyer-Peter Muller (MPM) transport model and variations of that model. The data show that negative dependencies ($p < 0$) are obtained for d_o and q_p, whilst positive dependencies ($p > 0$) are obtained for $\int u^3 dt$. This indicates that a given d_o and q_p transport less sediment as grain size increases, whereas transport increases with grain size for a given $\int u^3 dt$. The p value is found to be narrowly ranged, $0.5 \leq p \leq -0.5$. On average, the incorporation of a pressure gradient term via the piezometric head into the MPM formulation reduces q_p by 4% (fine sand) to 18% (coarse sand). The measured total transport for fine and coarse sands is best predicted using MPM and MPM + dp^*/dx respectively. However, the inferred optimum transport coefficient in the MPM formulation is about 30, much higher than the standard coefficient in a steady flow and this is not due to the presence of the pre-suspended sediment. The optimum transport coefficient indicates some sensitivity to grain size, suggesting that some transport processes remain unaccounted for in the model.

1. Introduction

Sand and shingle beaches exhibit median grain sizes that vary by approximately two orders of magnitude, between $D_{50} = 0.15$ mm and 20 mm. Research into the relationship between sediment transport and grain size under field conditions is rare because there are no significant changes of beach median grain sizes over regular time scales (days and months). Data exists for unsteady flows in the coastal literature, but this is for oscillatory flows in water tunnels, OWT (e.g. Dohmen-Janssen, 1999; O'Donoghue and Wright, 2004) or under surface waves (Dohmen-Janssen and Hanes, 2002; Kranenburg et al., 2013; Schretlen et al., 2011), and are limited mainly to sandy beaches with median grain sizes up to 0.5 mm. Few, if any, data exist for swash flows, which are physically different from an oscillatory flow. Oscillatory flows include added complications from phase lags and ripples, and the magnitude and period of the wave orbital velocity. For example, the net sediment transport measurements in a large scale water tunnel of Dohmen-Janssen (1999) revealed two opposite trends, a negative grain size dependency for sand up to $D_{50} = 0.35$ mm but a positive grain size dependency for $D_{50} \leq 0.22$ mm when the wave orbital velocity exceeded 1 m/s. Similarly, a negative grain size dependency is also found from the water tunnel measurements of O'Donoghue and Wright (2004) using $D_{50} \leq 0.5$ mm. For waves of similar velocity skewness, the presence of onshore streaming under surface waves can lead to an increase in the net transport rates for medium sand ($D_{50} \geq 0.2$ mm) and changes the transport direction from offshore directed to onshore directed.

To a great extent, the research on sediment transport with different grain sizes under oscillatory flow has focussed on several aspects; phase lags between velocity and sediment concentration, the thickness of the sheet flow layer, the apparent roughness height in the sheet flow layer (e.g. Dohmen-Janssen et al., 2001) and the influence of onshore streaming in surface waves (Dohmen-Janssen et al., 2001; Kranenburg et al., 2013), rather than on the influence of grain size directly. Nielsen and Callaghan (2003) were probably the first to suggest a way of quantifying the boundary layer streaming effect in flumes versus tunnels and their treatment was refined by Nielsen (2006). Processed based models (i.e. hydro-morphodynamic model) are more complex and theoretically

* Corresponding author at: School of Civil Engineering, University of Queensland, St Lucia, Brisbane, Queensland, 4072, Australia. Tel.: +61 733653767.
E-mail addresses: i.othman@uq.edu.au (I.K. Othman), t.baldock@uq.edu.au (T.E. Baldock), dave.callaghan@uq.edu.au (D.P. Callaghan).

0378-3839/$ – see front matter © 2013 Elsevier B.V. All rights reserved.
http://dx.doi.org/10.1016/j.coastaleng.2013.09.001

capture the grain size influence in unsteady flow by modelling the boundary layer, the vertical structure of the sediment concentration and turbulence diffusivity that feed back into the sediment transport calculation (e.g. Hassan and Ribberink, 2010; Kranenburg et al., 2013; Teakle, 2006). Note that some of the processed based models do not model the boundary layer directly (i.e. they use a fixed friction factor) and the grain size influence still depends on the empirical transport formulae adopted in the morphological module (Briganti et al., 2012; Kelly and Dodd, 2010; Postacchini et al., 2012).

Whilst run-up and overtopping in the swash zone are reasonably represented as a one dimensional flow (Young et al., 2010), no clear theory has emerged to explain how the transport rate and grain size are related (i.e. $q \propto D^p$, where q is total transport (m^3/m per swash) and D is a measure of grain size) in the swash zone. Indeed, there are no experimental data that explicitly consider the influence of grain size on swash zone sediment transport, albeit with wide acceptance that grain size influences beach morphology and the morphodynamics response (Masselink et al., 2010; van Rijn et al., 2007). The current transport models, largely derived from steady flow based on the Shields (1936) approach in terms of bed shear stress, have a positive dependency ($p \approx 1$) on grain size solely through the friction factor. Additionally, the widely applied CERC formula for longshore transport is also independent of grain size, although it has been argued (e.g. King, 2005; Van Wellen et al., 2000) that the constant in the CERC formula has an inverse grain size dependency, which mathematically yields $q \approx D^{-1}$. Similarly, the field-derived experimental value of the CERC constant also indicates a negative grain size dependency (Del Valle et al., 1993). To date, this effect cannot be seen directly from typical parametric or empirical sediment transport models (e.g. Sleath, 1984 pg 292), as it is always embedded in a friction factor (i.e. $\tau_b = 0.5\rho f u^2$) or some proportionality constant (e.g. Bailard and Inman, 1981) and the sediment transport results are frequently plotted in term of non-dimensional transport and Shields parameter. Note that there are also uncertainties in the proportionality constants appropriate for the swash zone, which may differ from steady flow values (Baldock et al., 2005; Hughes et al., 1997). This maybe for two reasons; the interlinking of the friction factor and the sediment transport coefficient, and the presence of pre-existing turbulence and pre-suspended sediment generated during bore collapse, which may increase the sediment transport.

Even for simpler steady flows, there is no consensus as to the influence of grain size on transport rate, with disagreement found across the riverine-sediment transport literature (see Martin and Church, 2000). The q–D correlation was originally introduced empirically by Bagnold (1980, 1986) using an inhomogeneous formula (i.e. with unbalanced dimensions). However, a contradiction exists between Bagnold's (1956) theory and his (1980; 1986) empirical correlations. The former support the Meyer-Peter Muller (MPM) transport relationship, with an additional constant dependent on D, but the latter demonstrated an inverse dependency, $q_b \propto D^{-1/2}$.

Owing to the uncertainty in the q–D dependency, the present study examines this dependency experimentally for a range of different parameters using an unsteady dam break flow. The p values are inferred for different flow parameters; the initial dam depth, d_o, the integrated depth averaged velocity, $\int u^3 dt$, and the predicted transport potential, q_p, using the Meyer-Peter and Muller (1948) transport model. The inferred dependency is intended for application to the beach face and might not be valid outside this zone when the non-linear effects of (bore) turbulence induced sediment pickup, sediment settling and phase lags becomes dominant (i.e. different physics occur).

The aim of the current study is to test the following hypotheses:

- Is the total transport dependent on grain diameter, for shallow sheet flow conditions typical of swash uprush? If yes, then is it proportional or inversely proportional, and to what power (i.e. $q \propto D^p$)?
- Is the difference in the sediment transport coefficient compared to steady flow caused by pre-suspended sediment?

This paper is structured as follow. Section 2 presents the experimental setup and test conditions, followed by the model-data comparisons of the experimental hydrodynamics in Section 3. Section 4 presents the results of the q–D dependency, examined for the different flow parameters and Meyer-Peter and Muller (1948) sediment transport model with/without pressure gradient and bed slope corrections. Final conclusions are given in Section 5.

2. Experimental setup and instrumentation

Idealised experiments simulating swash uprush overtopping a mobile sediment bed were conducted using a tilting dam break apparatus at the Seddon Hydraulics Laboratory, The University of Queensland (Fig. 1). The dam break flume is 3 m long, 0.4 m wide and 0.4 m height and has been used previously in a number of studies studying bed shear stress (Barnes and Baldock, 2010) and overtopping (Hogg et al., 2011) during swash-type dam break flows over initially "dry" fixed beds. The gate opening was performed manually using a pivoting arm and video analysis showed that the gate was fully opened to a height greater than 0.2 m in less than 0.12 s (Barnes, 2009), hence the opening can be considered as nearly instantaneous. In order to avoid and minimise leakage and resistance during gate opening, the gate sides and base were covered with silicon seals and a small amount of silicon grease. For the present experiments, the reservoir length was kept constant at 1 m, leaving a 2 m long section of mobile sediment bed downstream. In order to minimise seepage under the gate, and scour prior to gate opening, the reservoir section is fitted with a 2 cm thickness of acrylic false bed. Careful consideration was given to the intersection between the sand and the false bed to minimise significant scour once the gate is lifted and piping action from water leaking from the gate. Prior to each run, any water in front of the gate was removed using a pump and this, in conjunction with a 0.5 cm diameter drain hole just downstream from the gate, ensured a "dry" but saturated downstream sediment bed.

A 2 cm thick layer of sand was placed over the entire length of the downstream side of the gate, and levelled between each run with a 'T' shape profiler running on rails along the top of the flume to maintain an even surface throughout. Four different sediment sizes, with median grain sizes of $D_{50} = 0.22$, 0.5, 0.9 and 2.65 mm, and three bed slopes, $\tan\beta = 1/10$, 1/20 and 1/30, were used in the experiments. Since it is impossible to measure bed load and suspended load separately in such shallow and transient flows, the total sediment transport was measured by allowing the fluid and sediment to overtop the end of the flume, where it was collected. At the overtopping edge, sand was prevented from avalanching and maintained in place by a 2 cm height aluminium strip acting as a toe board. The toe board is designed not to protrude above the sand level so that the overwash processes is not affected. Since the bulk of the transport occurs during supercritical flow, the presence of the edge has a negligible impact on the sediment transport. Note that the same method was used by Baldock et al. (2005) in a wave flume to study overtopping and overwash due to wave run-up. The surface elevations and water depths were measured at 0.535 m, 1.235 m, 1.635 m, 1.775 m and 1.955 m downstream of the gate using Microsonic acoustic displacement sensors, Mic + 25/IU/TC (MS25) with accuracy ±1 mm, sampled at 50 Hz. These sensors have a response time of 32 ms and a sensing distance between 30 and 250 mm (Microsonic, 2010).

The experiments provide highly reproducible measurements with low initial free stream turbulence intensity and exclude pre-suspended sediment. The total transport, q_m, was measured by trapping the overtopped sediment using a removable sediment trap of 0.8 m length, 0.6 m width, 0.2 m height and a monofilament fabric filter of 0.043 mm aperture. The trap sits on the overtopping tank of 1.22 m length, 0.6 m width, 0.6 m height. The trap length was designed to cope with the trajectory of the overtopping sand–water mixture and the splashing is minimised using a 30 cm height plastic cover screwed on the frame at

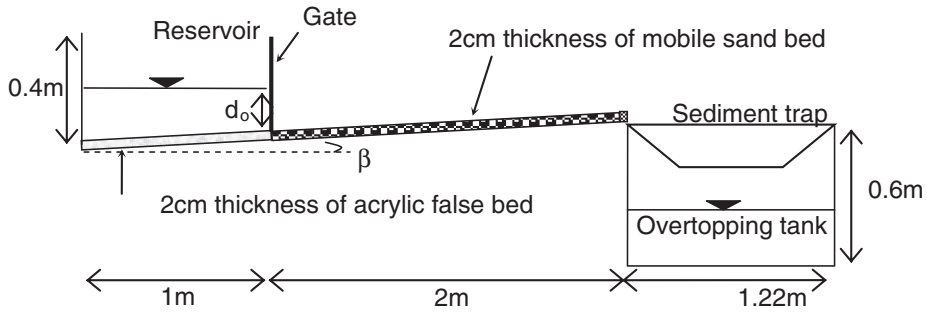

Fig. 1. Experimental setup.

the downstream end. After each test, the sand captured by the trap was measured by tipping and washing the collected sand into a measuring cylinder. The volumetric transport is measured by allowing the collected sediment to settle naturally under water in the measuring cylinder. The saturated sand volume can be converted to dry weight by drying the saturated sample if required. Experiments were performed for five different reservoir depths over three different bed slopes for each of the four grain sizes, yielding 60 test cases. A summary of the experimental cases is given in Table 1.

3. Hydrodynamic modelling

The very shallow flow immediately behind the moving leading edge of the dam break wave makes it very difficult to collect velocity data in the vicinity of the wave tip (Barnes, 2009), although the speed of the leading edge can be measured. Since the flow velocity is close to maximum in the tip region, this region of the flow transports a significant amount of sediment. Thus, measured flow velocities are not available for testing sediment transport models. Further, single point measurements of the flow velocity are dependent on the relative vertical location within the boundary layer and therefore do not provide a consistent representative velocity (see Puleo et al., 2000). Hence, the present study used the depth averaged velocity, predicted using a finite volume model, *TUFLOWfv*, calibrated against the measured flow depth (Fig. 2), the overtopping volume, and the wave tip celerity (Fig. 3). Herein, all calculations are performed using the calibrated velocities unless otherwise stated.

TUFLOWfv is a depth averaged finite volume model that solves the non-linear shallow water equation (NLSWE) using the assumption of hydrostatic pressure. The model features an irregular flexible mesh which allows quadrilateral and/or triangular cell discretisation and a wetting depth, a parameter that controls when the cells are considered as 'wet' so that the mass and momentum fluxes are calculated. The wetting depth was set to 1 mm, since a lower value did not show significant differences in the predicted depths, less than 3 mm, and the accuracy of the flow depth measurement is also 1 mm. The model has been tested against wide range of flows; for benchmark tests and publications refer to Néelz and Pender (2010).

Typical time series of the measured and predicted velocity and flow depth are given in Fig. 2. The leading and trailing edges of the flow depth are well predicted but the reflected waves, indicated by the hump in the plot, occurred slightly later than predicted. The reflected waves occurred as a result of the negative wave propagating upstream from the dam break and reflecting from the end wall. This is modelled by *TUFLOWfv* and included in the predicted velocity.

A good agreement is achieved between the measured and predicted overtopping volume, and to a slightly lesser agreement, within a ±20% error band, with the measured tip celerity and the maximum predicted depth averaged velocity (Fig. 3). The wave tip is considered arrived at a sensor when the measured depth is greater or equal to 2 mm and the tip celerity is calculated from the last two sensors prior to the edge (1.775 m and 1.955 m downstream of the gate).

Table 1
Experimental data.

tan β	Initial water depth, d_o, (m)	Median grain size, D_{50}, (mm)
1/10	0.20, 0.22, 0.23, 0.24, 0.25	0.22, 0.5, 0.9 and 2.65
1/20	0.12, 0.14, 0.16, 0.18, 0.20	0.22, 0.5, 0.9 and 2.65
1/30	0.10, 0.12, 0.14, 0.16, 0.18	0.22, 0.5, 0.9 and 2.65

4. Results

4.1. Grain size dependency

If q is assumed as a function of D only and keeping other parameters constant (i.e. $q \propto D^p$), the grain size dependency can be deduced following King (2005):

$$q_m \propto D^p F \tag{1}$$

$$F = \left[d_o, \boldsymbol{U}^3, q_p\right] \tag{2}$$

$$\frac{q_m}{F} = D^p = m \tag{3}$$

$$p = \frac{\log(m_1/m_2)}{\log(D_1/D_2)} \tag{4}$$

where d_o, $\mathbf{U}^3$, q_m and q_p are the initial reservoir depth, integrated depth averaged velocity cubed measured total transport and predicted total transport respectively (defined in Sections 4.2 to 4.4). m_1 and m_2 can be obtained from the measured total transport, q_m, from two different swash events, with different grain sizes with $D_1 < D_2$ but otherwise constant forcing conditions. The p value can be calculated for every particular forcing term, F, e.g. d_o or q_p. However, this would be noisy because of measurement accuracy and non-perfect repeatability. An average value of p is required for each forcing parameter and each pair of grain sizes. Therefore, the p value is calculated using the variation in q_m for a given forcing parameter. The variation in q is obtained from the slope of the regression lines, m, from plotting q_m versus the forcing parameter for a range of flow conditions.

To date, there is no definite formula to calculate p and the current approach gives a simple relationship. Eq. (1) could be used by comparing q_1 and q_2 under similar flow conditions, i.e. for the same Shields number, $\theta_1 = \theta_2$ (King, 2005). However, for unsteady flow, θ is not constant over the duration of each test. Consequently, θ cannot be used as the forcing parameter as in King (2005) or Nielsen (1992). Hence, this section investigates the grain size dependency viewed from three different perspectives using the following forcing parameters: the initial bore height, d_o; the time integrated depth averaged velocity, $\boldsymbol{U}^3 = \int u^3 dt$; and the time integrated predicted total transport, q_p, calculated using Shields type formulae. The Shields type formulae tested herein are in

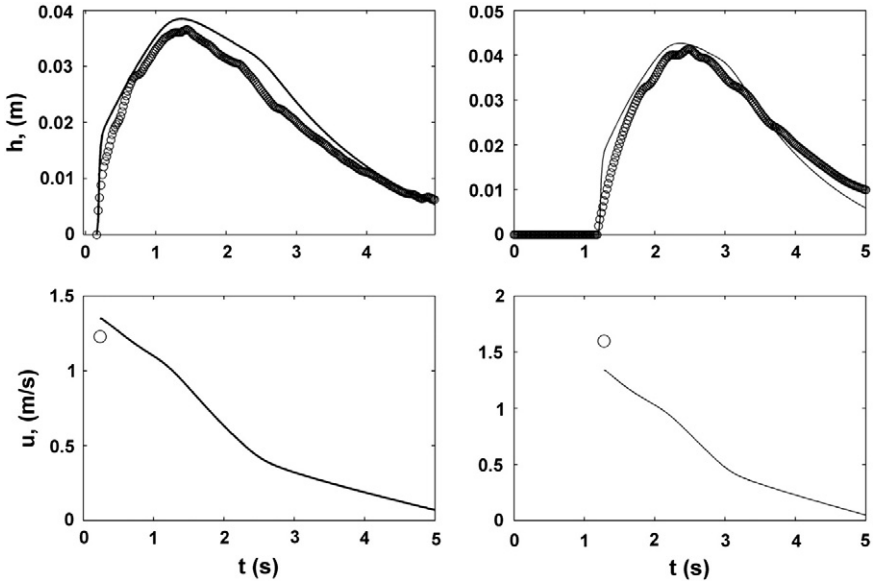

Fig. 2. Measured (symbols) flow depth, h, and modelled (lines) average horizontal velocity, u, at $x = 1.955$ m downstream of the gate for $D_{50} = 0.22$ mm on $\tan\beta = 1/20$ (right), $d_o = 0.20$ m and $\tan\beta = 1/30$ (left), $d_o = 0.18$ m. Circles in bottom panels are the measured tip celerity of the leading edges.

the form of Meyer-Peter Muller (MPM); MPM with pressure gradient correction calculated using the piezometric head (MPM + dp^*/dx); MPM with a bed slope correction to the Shields parameter (MPM + θ correction); MPM with pressure gradient correction and bed slope correction (MPM + dp^*/dx + θ correction); MPM with incorporation of local acceleration and phase shift (Nielsen, 2002); MPM with time varying friction factor, $f(t)$, through the Colebrook–White formulation (MPM_CW) and with a time varying f through the Colebrook–White formulation with dp^*/dx (MPM_CW + dp^*/dx). The influence of the pressure gradient is also discussed in detail with some examples.

The legends in all of the figures follow the same convention, with different symbols indicating different bed slopes, tan β, and different colours signifying different grain sizes, D_{50}, unless otherwise stated.

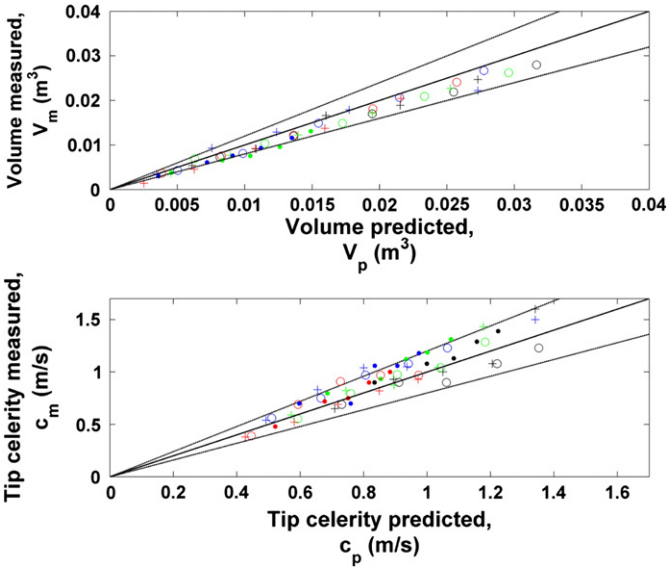

Fig. 3. Measured and predicted overtopping volume (top) and wave tip celerity (bottom). $D_{50} = 0.22$ mm (black), 0.5 mm (green), 0.9 mm (blue) and 2.65 mm (red) on $\tan\beta = 1/10$ (·), 1/20 (+) and 1/30 (°). Solid thick line is 1:1 line and the lines above and below the solid line are ±20% error bands.

For readability, $D_{50} = 0.22$, 0.5, 0.9 and 2.65 mm are described as fine, intermediate, medium and coarse sands, respectively. Whenever convenient, when comparing the dependency between two grain sizes, for example between fine and medium sand, the short form of fine–medium sand is used. The dependencies (p values) and the transport coefficients for the whole dataset are summarised graphically at the end of the paper.

4.2. Total transport versus initial reservoir depth, d_o

The initial depth of the reservoir, d_o, can be interpreted as a measure of the initial strength of the dam break wave when the water is released from the static condition, causing the potential energy to be converted to kinetic energy, driven by a strong initial pressure gradient, dp/dx. For inviscid and hydrostatic conditions, the initial velocity of the leading edge is proportional to the square root of the initial depth.

Taking the initial depth, d_o, as the controlling parameter, Fig. 4 shows an inverse q–D relationship in which total sediment transport increases with a decrease in grain size (i.e. negative p). The negative dependency for d_o is expected from frictional effects, as indicated by the lower modelled velocity for larger grain sizes (i.e. Fig. 2). The data are very consistent between grain sizes, with regression coefficients very close to unity, with a near perfect linear relationship between the total transport and the initial depth.

Only the fine sand data show significant differences in the gradient of the regression lines but the intermediate, medium and coarse sand data lie close together and some of them overlap at lower depths. This in turn creates mixtures of small positive/negative q–D dependencies at lower depths between these sands, but stronger negative dependencies between fine sand and the other sands. The negative dependency increases as the bed slopes decreases and the calculated p value ranges from −0.7 to 0.19. The linear regression equations and the associated R^2 are specified in Table 2.

4.3. Total transport versus integrated depth averaged horizontal velocity cubed, $\int u^3 dt$

Unlike the steady flow or oscillatory flow data, the dam break swash flow does not have corresponding time-averaged velocity amplitude to relate to the measured transport, nor does it have a representative

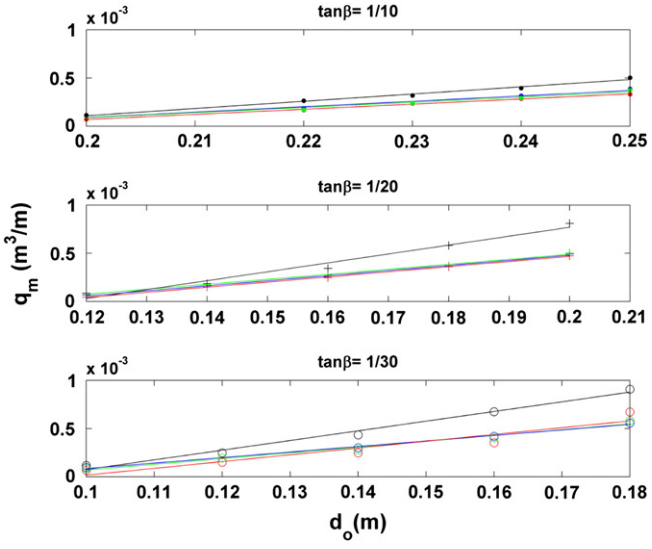

Fig. 4. Measured transport, q_m, against d_o for D_{50}0.22 mm (black), 0.5 mm (green), 0.9 mm (blue) and 2.65 mm (red) on tan $\beta = 1/10$ (·), 1/20 (+) and 1/30 (°).

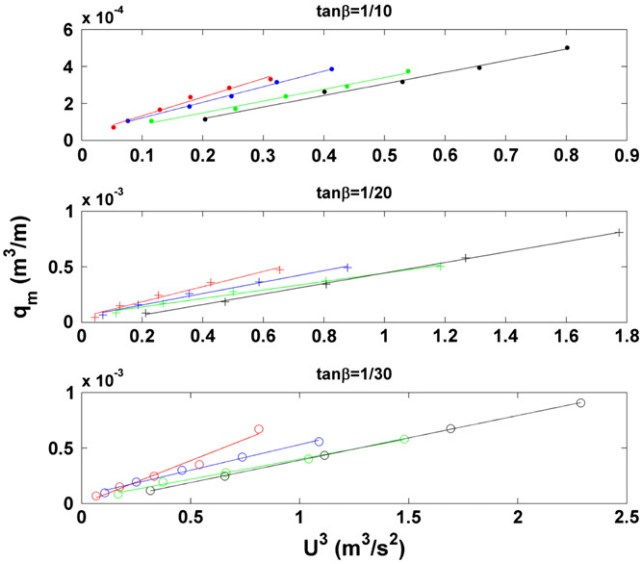

Fig. 5. Measured transport, q_m, against $\mathbf{U}^3$ for $D_{50} = 0.22$ mm (black), 0.5 mm (green), 0.9 mm (blue) and 2.65 mm (red) on tan $\beta = 1/10$ (·), 1/20 (+) and 1/30 (°).

velocity. Hence, here, the influence of velocity is inferred through the sum of the depth averaged instantaneous horizontal velocity cubed just upstream from the overtopping edge ($x = 1.955$ m):

$$\boldsymbol{U}^3 = \int_{t=u_{max}}^{t=u>u_{cr}} u^3 dt \tag{5}$$

$$u_{cr} = \sqrt{(s-1)gD\theta_{cr}}, \tag{6}$$

where u_{cr}, $s = 2.65$, $g = 9.8$ m/s^2 and θ_{cr} are critical velocity, specific gravity of sand, gravity, and critical Shields parameter respectively. The values of θ_{cr} used in the calculation are discussed in Section 4.2 below. Note that although $\mathbf{U}^3$ has units of m^3/s^2, we regard it as analogous to u^3 in conventional sediment transport models.

The data in Fig. 5 demonstrate a linear relationship with $\mathbf{U}^3$ and increasing transport at larger D_{50} for a given $\mathbf{U}^3$ (i.e. positive dependency), in contrast to the relationship with d_o. This is associated with the monotonically decreasing velocity (as a result of greater friction) and reduced overtopping durations as grain size increases. Considering the fluid and sediment transport as an advective process, in order to obtain the same $\mathbf{U}^3$ at the edge with greater friction, a larger initial reservoir depth is required. Further, friction takes time to act, so for a given $\mathbf{U}^3$ at the edge, the velocity close to the gate will be larger for larger grain size. Consequently, proportionately greater sediment pickup occurs, leading to proportionately larger total sediment transport. The grain size dependence from the swash observations of this study agrees closely with that indicated by Del Valle et al. (1993) for total littoral drift. The linear regression equations and the associated R^2 are given in Table 4 and the calculated p values ranges from 0.02 to 0.5. Further, the data indicate that the total transport reduces on mild bed slopes (Table 4). Again, this is because to obtain the same $\mathbf{U}^3$ at the edge for a milder bed slope requires a smaller initial d_o. A smaller d_o results in a lower initial velocity and less sediment pickup, and consequently smaller total transport.

4.4. Measured total transport versus predicted total transport potential

The critical slope correction, θ_{cr}, is also included in the predicted total transport, q_p, to account for the threshold of motion for a particle on a slope, where particles on a downward slope will be easily more dislodged and vice versa. θ_{cr} is given below, derived from a force balance in air via the Coulomb Law as explained and proposed by Fredsoe and Deigaard (1992):

$$\theta_{cr} = \theta_{cr\beta=0}\left(1 \pm \frac{\tan\beta}{\tan\alpha}\right)\cos\beta \tag{7}$$

where $\tan\beta$ and $\tan\alpha = 0.63$ ($\alpha = 32.2^{\circ}$) are the bed slope and angle of repose of sediment, respectively. The critical Shields value on a horizontal bed, $\theta_{cr\beta=0}$, is estimated from the Shields diagram, following the proposed formulae of Van Rijn (1993):

$$\theta_{cr\beta=0} = \begin{cases} 0.14{D_*}^{-0.64}, & 4 < D_* \le 10 \\ 0.04{D_*}^{-0.1}, & 10 < D_* \le 20 \\ 0.013{D_*}^{0.29}, & 20 < D_* \le 150 \end{cases} \tag{8}$$

where $D_* = [g(s-1)/\nu^2]^{1/3} D_{50}$ and $\nu = 10^{-6}$ m^2/s are dimensionless grain size and kinematic viscosity of water at 20 °C, respectively. The inclusion of the bed slope correction increases θ_{cr} by approximately 15%, 8% and 5% for $\tan\beta = 1/10$, 1/20 and 1/30 correspondingly, compared to the horizontal bed values. θ_{cr} values used in the calculations are summarised in Table 3. The linear regression equations and

Table 2
Linear regression for d_o.

tan β	Linear regression equation, y=; R^2							
	$D_{50} = 0.22$ mm		$D_{50} = 0.5$ mm		$D_{50} = 0.9$ mm		$D_{50} = 2.65$ mm	
1/10	0.0075*X*-0.0014	0.99	0.0054*X*-0.001	0.97	0.0056*X*-0.001	0.98	0.0053*X*-0.001	1
1/20	0.0092*X*-0.0011	0.98	0.0052*X*-0.0005	0.99	0.0053*X*-0.0006	1	0.0053*X*-0.0006	1
1/30	0.01*X*-0.0009	0.99	0.006*X*-0.0005	0.98	0.0057*X*-0.0005	1	0.007*X*-0.0007	0.9

Table 3
Values of θ_{cr} used in transport calculations.

D_{50} (mm)	D_* (−)	$\theta_{cr\,\beta=0}$	tan β	θ_{cr}
0.22	0.51	0.047	1/10	0.0542
			1/20	0.0507
			1/30	0.0495
0.5	2.52	0.031	1/10	0.0357
			1/20	0.0334
			1/30	0.0326
0.9	2.53	0.032	1/10	0.0369
			1/20	0.0345
			1/30	0.0337
2.65	6.33	0.044	1/10	0.0507
			1/20	0.0474
			1/30	0.0463

the associated R^2 for variations of the MPM model (discussed below) are summarised in Table 5.

4.4.1. Meyer-Peter and Muller (1948), MPM

The predicted transport potential using the original form of the MPM formula is evaluated with the friction factor, $f_{2.5}$, and Shields parameter, θ, calculated based on those proposed for unsteady flows by Nielsen (1992):

$$\frac{q_b}{\sqrt{(s-1)gD^3}} = C(\theta-\theta_{cr})\sqrt{\theta} \tag{9}$$

$$q_p = \int q_b dt \tag{10}$$

$$\theta = \frac{0.5\rho f u^2}{\rho(s-1)gD} \tag{11}$$

$$f_{2.5} = \exp\left[5.5\left(\frac{2.5D_{50}}{A_{rms}}\right)^{0.2} - 6.3\right] \tag{12}$$

where q_b, q_p, $A_{rms} = \frac{\sqrt{2}}{\omega_p}\sqrt{\mathrm{Var}\{u(t)\}}$, $\omega_p = \frac{2\pi}{T}$, $C = 12$ and $f_{2.5}$ are sediment transport rate (m^2/s), total sediment transport (m^2), wave orbital amplitude, peak angular frequency, transport coefficient, and wave friction factor respectively. By combining Eqs. (9), (11) and (12), the MPM formula gives an approximately linear dependency between transport and grain size, arising only through the friction factor. Thus, for a similar flow velocity the MPM formulation shows a positive q–D relation (Fig. 6) with $p \approx 1$ for $D_{50} > 0.5$ mm.

The predicted total transport calculations are performed using the calibrated model velocities and are compared with the measured data. Fig. 7 demonstrates that the standard MPM model underpredicts the measurements. The data for intermediate, medium and coarse sands are close to each other despite the large difference in grain sizes, but still discernible. The regression lines for the sloping bed data (except for the fine sand) have a very small y intercept, $\leq 10^{-5}$ (not included in Table 3), suggesting a close prediction of θ_{cr}. The linear regression equations and the associated R^2 are given in Table 5 and the calculated p value ranges from −0.08 to −0.6. Since the pressure gradient is not accounted in the standard MPM model and can be important in an unsteady flow, the next section explores the influence of including a pressure gradient correction.

4.4.2. Meyer-Peter and Muller (1948), MPM with pressure gradient, dp^*/dx, correction

Sediment transport at the very front of the uprush could possibly be influenced by strong landward pressure gradient forces associated with very localised strongly landward dipping surface shapes at the tip. This would be somewhat similar to what was described in Khezri and Chanson (2012) who observed strong bursts of sediment transport associated with the passage of bore fronts. Sediment transport measurements under oscillatory flow (Flores and Sleath, 1998) and skewed waves (e.g. Watanabe and Sato, 2004) have shown that the pressure gradient, dp^*/dx, enhances onshore transport. The concept was later adopted for the swash using the local acceleration, $\partial u/\partial t$, as a proxy to dp^*/dx (e.g. Nielsen, 2002; Puleo et al., 2003). Unfortunately, field observations of Baldock and Hughes (2006) and numerical calculations by Puleo et al. (2007) have shown that $\partial u/\partial t$ is a very poor proxy for the pressure gradient because the swash run-up flow decelerates for most of the run-up. Similarly, a recent laboratory investigation using state of the art Bubble Image Velocimetry (Pedrozo-Acuña et al., 2011) shows that there is only a weak correlation between local acceleration and pressure gradient in the swash zone (Baldock, 2012). Therefore, instead of using Eulerian measurements of local flow acceleration, the present study used the surface elevation, η, to infer the pressure gradient (i.e. $dp^*/dx = -\rho g(d\eta/dx)$, where dp^*/dx is the piezometric pressure gradient). Barnes and Baldock (2010) show this is a good approximation in the same experimental arrangement. The approach is a correction to the Shields parameter, accounting for the pressure gradient force as an additional stress, as proposed by (Nielsen, 1992), which is written here as:

$$\theta_{PG} = \frac{0.5\rho f u^2 + \rho g\left(\frac{d\eta}{dx}\right)D}{\rho(s-1)gD} \tag{13}$$

The dp^*/dx term is calculated using a hydrostatic assumption (Baldock and Hughes, 2006) inferred from the measured surface elevation between 2 consecutive sensors close to the overtopping edge at $x = 1.775$ m and 1.955 m (i.e. $dp^*/dx = -\rho g((\eta_2 - \eta_1)/\Delta x)$) as illustrated in Fig. 8. Calculations are restricted to periods when $\theta_{PG} > \theta_{cr}$. dp^*/dx is negative if the free surface is dipping toward the reservoir (i.e. generating a reduction in bed shear stress, τ_b) and vice versa. Consistent with the previous observations of Baldock and Hughes (2006) and Barnes and Baldock (2010), on an upward sloping bed the pressure gradients even at the wave front are small and typically negative. Even where pressure gradients are positive, they are less than 0.1 N/m^2, which is unlikely to impact on sediment transport rates (Baldock and Nielsen, 2010).

Fig. 9 illustrates the typical time series of measured depth and the associated modelled depth averaged horizontal velocity, u, for tests with an initial depth of 0.2 m. The measured depths are similar for both grain sizes and velocities are smaller for the coarse sand compared to the fine sand. The velocity and flow duration increase as the beach slope reduces. Fig. 10 illustrates the potential influence of the pressure gradient for the fine and coarse grains, where dp^*/dx is negative for the sloping beds for the majority of the flow duration. The ratio of the inertia force and drag force, $F_p/F_d = -\rho g(d\eta/dx)D/(0.5\rho f u^2)$ in Fig. 10 is calculated only for $\theta_{PG} > \theta_{cr}$, which limits the influence of dp^*/dx in the sediment transport calculations to the period of sediment motion.

Table 4
Linear regression for $\mathbf{U}^3$.

tan β	Linear regression equation, $y=$; R^2							
	$D_{50} = 0.22$ mm		$D_{50} = 0.5$ mm		$D_{50} = 0.9$ mm		$D_{50} = 2.65$ mm	
1/10	0.0006X	0.99	0.0006X	0.99	0.0008X	1	0.001X	0.98
1/20	0.0005X	1	0.0004X + 0.0001	0.99	0.0005X + 0.0001	0.99	0.0007X	0.98
1/30	0.0004X	1	0.0004X	0.99	0.0005X + 0.0001	0.99	0.0008X	0.98

Table 5
Linear regression for q_p at x = 1.955 m on tan β = 1/10, 1/20 and 1/30.

Method	Linear regression equation, $y=$; R^2							
	D_{50} = 0.22 mm		D_{50} = 0.5 mm		D_{50} = 0.9 mm		D_{50} = 2.65 mm	
MPM	3.49X − 0.0001	0.99	2.13X	0.99	2.1X	0.98	1.85X	0.84
MPM + dp/dx	3.48X	0.98	2.04X	0.97	2.15X	0.98	1.84X + 0.0001	0.92
MPM + θ correction	3.56X	0.98	2.29X + 0.0001	0.96	2.48X + 0.0001	0.94	3.64X + 0.0001	0.9
MPM + dp^*/dx + θ correction	3.55X	0.97	2.18X + 0.0001	0.94	2.48X + 0.0001	0.92	3.17X + 0.0001	0.82
Nielsen (2002)	91.26X + 0.0001	0.91	61.26X + 0.0001	0.88	67.56X + 0.0001	0.83	[a]384.75X + 0.0002, 118.91X	[a]0.95, 0.75
MPM_CW	2.91X	0.92	1.71X + 0.0001	0.91	2.22X + 0.0001	0.93	3.11X + 0.0001	0.93
MPM_CW + dp^*/dx	2.88X	0.91	1.59X + 0.0001	0.87	2.18X + 0.0001	0.89	2.66X + 0.0001	0.83

[a] for tan β = 1/10 only.

Note that the positive pressure gradient that occurred as the flow reaches sensors 1 and 2 corresponds to approximately a 2–3 mm difference in the water elevation between the sensors, which is within the measurement accuracy. The pressure gradient also fluctuates occasionally from negative to positive during the flow, particularly for coarse sand, but becomes negative again towards the end of the flow. Fig. 11 illustrates the total transport calculated via MPM and MPM + dp^*/dx correction. On average, the total contribution from the pressure gradient reduces q_p by 3% (fine sand) to 18% (coarse sand) which is visible through Fig. 11. However, whilst this correction does not significantly alter the overall regression coefficients (Table 5), it does improve the correlation coefficient for the coarse sand.

On a separate point, if $\partial u/\partial t$ is adopted as a proxy for dp^*/dx, the flow at a point commences at a maximum velocity, which is approximately the wave's tip celerity (i.e. $u_{max} \approx c_{tip}$). If the calculations start beforehand, this will result in a large imaginary acceleration at the start of the flow. Additionally, using $\partial u/\partial t$ as a proxy to dp^*/dx can be erroneous in the swash zone because often $u\,\partial u/\partial x \gg \partial u/\partial t$ (Puleo et al., 2007) and $\partial u/\partial t$ is always negative whilst $d\eta/dx$ varies (Baldock and Hughes, 2006). The sign of $\partial u/\partial t$ is important in the magnitude of the transport predicted by the Nielsen (2002) model, which is also discussed later.

4.4.3. *Meyer-Peter and Muller (1948) with bed slope correction*

The presence of a sloping beach suggests the need to have a bed slope correction for θ. Therefore, from a force balance between the shear stress and the sloping gravitational components, the bed slope correction can be expressed as (Nielsen, 2002):

$$\theta = \frac{\theta_{\beta=0}}{\cos\beta} \mp \tan\beta \tag{14}$$

However, the movement of particles in a sheet flow is essentially via the fluid-sediment suspension within an intense bed load layer (e.g. Sumer et al., 1996) and supported by a viscous force or an intergranular force (i.e. viscous or inertia region) (Bagnold, 1956). If the viscous force dominates over the intergranular force, particles motion is mainly supported by the fluid and hence transport would not be greatly affected by the bed slope. This questions the need to add any bed slope correction at all to the standard Shields parameter for a horizontal bed, $\theta_{\beta=0}$. The measured flow by itself should accommodate its surrounding environment, and perhaps including the bed slope correction on $\theta_{cr\beta=0}$ and dp^*/dx is sufficient. Consistent with this argument, the predicted/measured total transport without the bed slope correction in Fig. 7 indicate only subtle bed slope effects between the data from different bed slopes.

Note that the application of Eq. (14) decreases the average value of θ by approximately 49%, 37% and 31% for tan β 1/10, 1/20 and 1/30 respectively. These values seem quite large for corrections. Further, since the ratio of cos β is of the order one for tan β = 1/10 to 1/30, then whenever $\theta_{\beta=0} <$ tan β, θ becomes negative in the uprush, which is unrealistic. Consequently, the impact of the bed slope correction leads to further underpredictions, with 3 out of 15 (20%) coarse sand data points having $q_p = 0$, resulting in significant scatter (Fig. 12).Weaker inverse grain size dependencies are achieved between smaller grains and positive dependencies occur between the smaller-coarse grains as the gradient of the regression line for coarse sand is steepened. Furthermore, if the bed slope has a significant impact, including a bed slope correction should bring the data from different bed slopes on one line. However, from Fig. 13, the bed slope correction does not collapse the data onto one line, although there is decreased scatter as a result of the reduced values of q_p. The bed slope correction reduces the predicted total transport at the overtopping edge with increasing tan β, but for small grains the changes are small. However, there are complications introduced by sediment advection. That is, in order to get the same $\mathbf{U}^3$ or q_p at the edge for milder bed slope requires a smaller initial d_o. This gives lower initial velocity, less sediment pick up over the region of the bed prior to the edge and

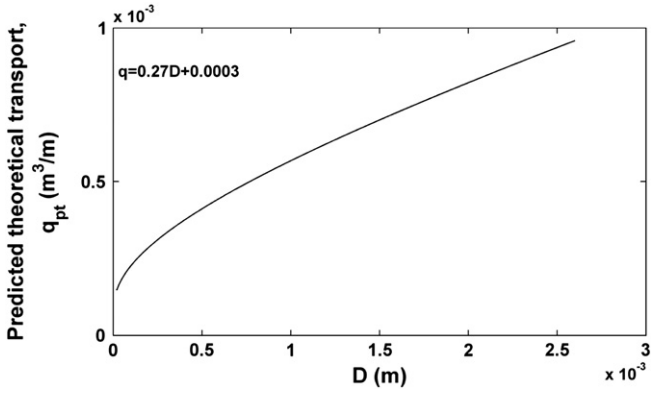

Fig. 6. Predicted theoretical transport, q_{p_t}, against grain size, D, using MPM on tan β = 1/30, d_o = 0.18 m.

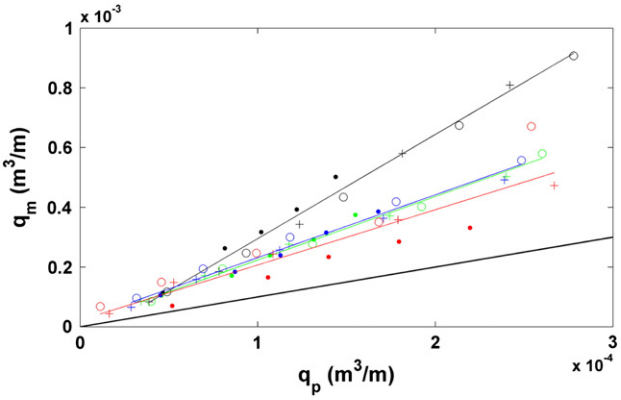

Fig. 7. Measured against predicted transport, q_p, using MPM for D_{50} = 0.22 mm (black), 0.5 mm (green), 0.9 mm (blue) and 2.65 mm (red) on tan β = 1/10 ( ), 1/20 (+) and 1/30 (°). Solid line is 1:1 line.

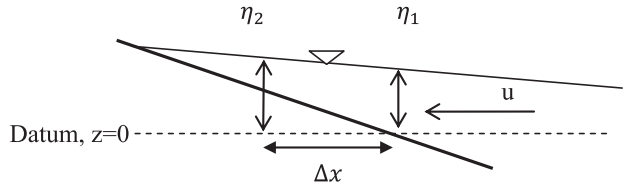

Fig. 8. Pressure gradient convention using piezometric head for the present study. Slope shown corresponds to a positive surface slope, or a negative (adverse) pressure gradient acting on sediment grains.

smaller total transport. Thus, the bed slope correction takes no account of the advective nature of the transport and only considers local conditions.

4.4.4. Meyer-Peter and Muller (1948) with dp^*/dx and bed slope correction

Comparing the bed slope correction and dp^*/dx, the former has a stronger influence on the transport predictions since the bed slope correction alters θ directly, as opposed to dp^*/dx which depends on the flow condition and usually has a smaller magnitude. Including both corrections decreases q_p and further aggravates the offset of the y intercept which suggests the corrections are not particularly beneficial (Fig. 13). Although the incorporation of both corrections manages to collapse the data slightly closer than the prediction with only dp^*/dx (Fig. 13), the error between the measured and the predicted transport potential increases, particularly for the medium and coarse sands, as demonstrated in Table 6. The reason is that the magnitude of the bed slope correction reduces all predicted values. Consequently, the negative p values increase slightly between fine, medium and intermediate sands, and the positive p values decrease between intermediate–coarse sand and medium–coarse sand, compared to the p values in previous section using MPM with the Shields bed slope correction only.

4.4.5. Nielsen (2002) model

Nielsen (2002, 2006) and Nielsen and Callaghan (2003) have suggested a modified version of the MPM formula that incorporates the pressure gradient in the form of a local acceleration and additional phase lag, φ_τ, between free stream velocity and sediment concentration. The phase lag is needed to take into account the differing fluid acceleration in asymmetric waves. The formula generates the sediment mobilising velocity in the form of:

$$u_\theta(t) = \sqrt{\frac{1}{2} f_{2.5}}\cos\varphi_\tau u + \sin\varphi_\tau \frac{\partial u/\partial t}{\omega} \tag{15}$$

$$\theta(t) = \frac{\tau_b}{\rho(s-1)gD_{50}} = \frac{u_\theta^2(t)}{(s-1)gD_{50}} \tag{16}$$

The value of φ_τ varies 37.5° and 51° (Nielsen, 2002; Nielsen and Callaghan, 2003). In the present calculation, $\varphi_\tau = 45^\circ$ is used based on the maximum φ_τ obtained in Nielsen (2002) using the swash data of Masselink and Hughes (1998). If φ_τ is set to 0° (transport is drag dominated), then Eq. (16) reduces to Eq. (11).

Applying this formula resulted in the extreme underprediction of the total transport, by an order of magnitude for fine sand, to two orders of magnitude for coarse sand (Table 5 and Fig. 16). This issue with the use of local acceleration was also pointed out by Baldock et al. (2005). Consequently, 4 out of 15 (27%) tests give $q_p = 0$ as $\theta \ll \theta_{cr}$. These tests have been excluded in Fig. 16 for better regression estimates. The reason for $q_p = 0$ is because $\partial u/\partial t$ is negative, thus reducing the representative velocity component, $\cos\varphi_\tau u + \sin\varphi_\tau (\partial u/\partial t)/\omega$ (Fig. 14) by approximately 3 times, and $\theta(t)$ (Fig. 15), and $q(t)$ correspondingly.

The data do not show marked differences between grain sizes at lower transport rates but differences are discernible at larger transport rates (Fig. 16). The negative dependencies are demonstrated in Fig. 16, where the gradient of the regression line for fine sand is steeper than the other grain sizes, excluding the coarse sand. The coarse sand data show scatter for different bed slopes with this model, which does not occur with the previous model.

In an attempt to maintain the reliability of the estimated dependency, p values are calculated only if $R^2 > 0.8$. Thus, calculations for coarse sand on tan $\beta = 1/10$ (dots in Fig. 16) are excluded because of the poor predictions. The maximum negative dependency, $p = -0.49$ is found between fine–intermediate sand and intermediate–medium sand, respectively. The dependency with respect to coarse sand on tan $\beta = 1/20$ and $1/30$ becomes positive with a maximum of $p = 0.27$

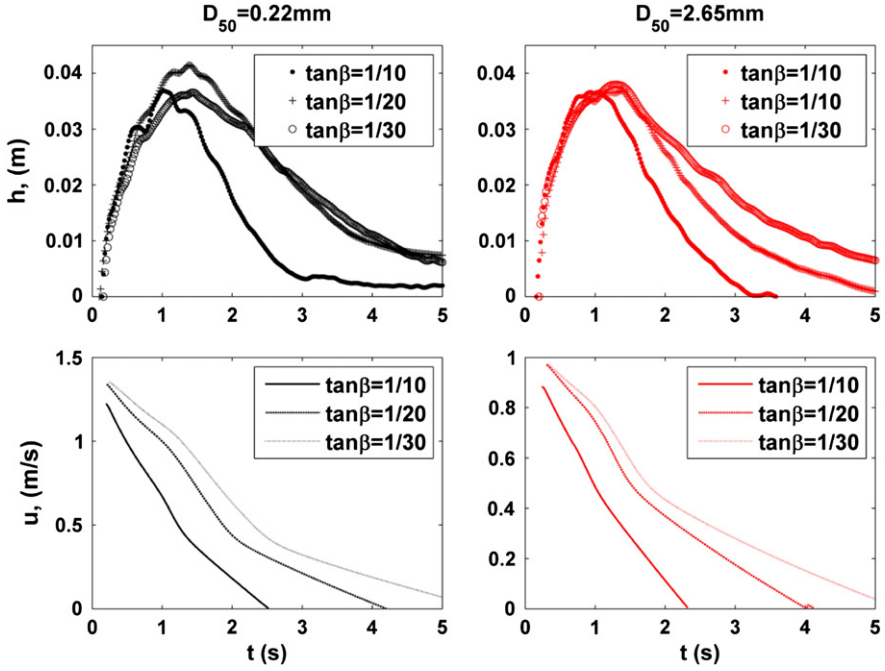

Fig. 9. Measured (symbols) flow depth, h, and modelled (lines) average horizontal velocity, u, at $x = 1.955$ m downstream of the gate for uprush. $d_o = 0.25$ m, 0.20 m and 0.18 m on tan $\beta = 1/10$, 1/20 and 1/30 respectively.

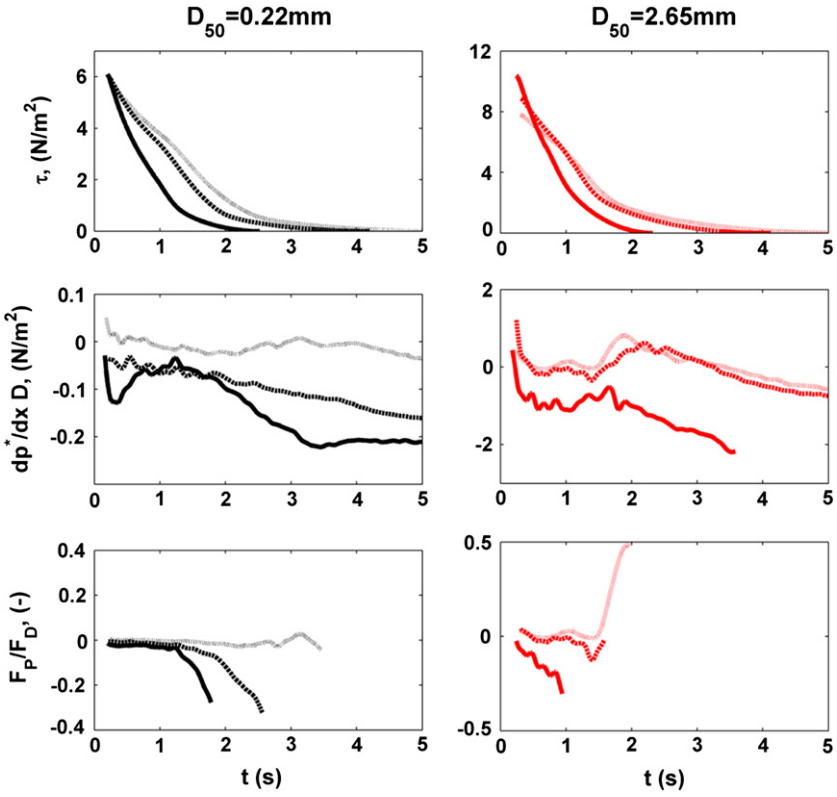

Fig. 10. Ratio of pressure gradient to drag force, $F_p/F_d = (dp^*/dxD)/(0.5\rho f u^2)$, for $D_{50} = 0.22$ mm (left panels) and $D_{50} = 2.65$ mm (right panels). $d_o = 0.25$ m on tan $\beta = 1/10$ (-), $d_o = 0.20$ m on tan $\beta = 1/20$ (–) and $d_o = 0.18$ m on tan $\beta = 1/30$ (…).

between medium–coarse sand, as the slope of the regression line for the coarse sand is much steeper.

4.4.6. *Meyer-Peter and Muller (1948), with time varying friction via Colebrook–White*

Given that both the Reynolds number and relative roughness change during the swash flow, the use of a constant friction factor is an approximation. Barnes and Baldock (2010) showed that friction factors vary during these dam break flows by approximately a factor 2. Consequently, the calculation of q_p using a time varying friction factor based on the modified Colebrook–White equation (Swamee and Jain, 1976) is presented. The purpose of these calculations is to see whether or not the influence of a time varying friction factor is likely to be significant enough to change the inferred grain size dependency. The time varying friction factor is calculated as:

$$f = \frac{1}{16\left[\log_{10}\left(\frac{k_s}{3.7D_h} + \frac{2.51}{Re^{0.9}}\right)\right]^2} \tag{17}$$

where $\mathrm{Re} = uD_h/\upsilon$, $D_h = 4A/P$, $k_s = D$, A and P are Reynolds number, hydraulic depth, bottom roughness, wetted area and wetted perimeter

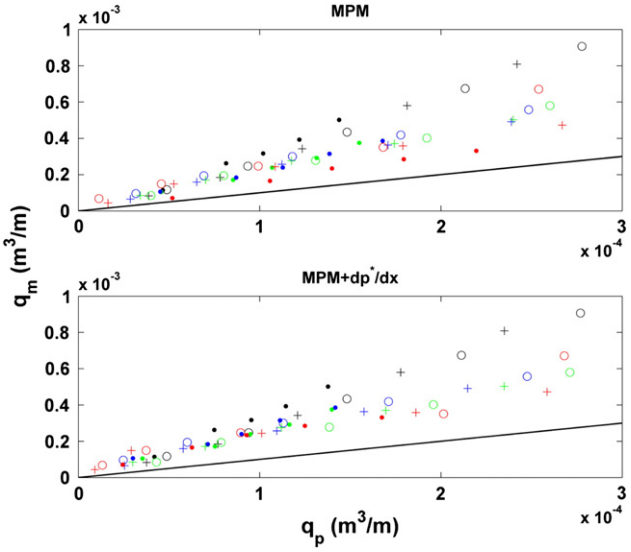

Fig. 11. Measured versus predicted transport, q_p, using MPM (top) and MPM with dp^*/dx (bottom) for $D_{50} = 0.22$ mm (black), 0.5 mm (green), 0.9 mm (blue) and 2.65 mm (red) on tan $\beta = 1/10$ (.), 1/20 (+) and 1/30 (o). Solid line is 1:1 line.

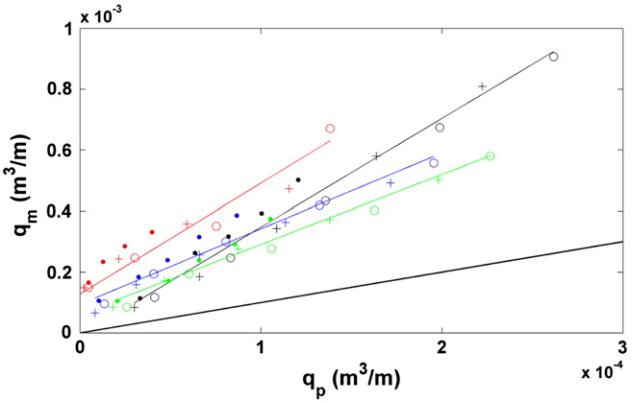

Fig. 12. Measured versus predicted transport, q_p, using MPM with bed slope correction for $D_{50} = 0.22$ mm (black), 0.5 mm (green), 0.9 mm (blue) and 2.65 mm (red) on tan $\beta = 1/10$ (.), 1/20 (+) and 1/30 (o). Solid line is 1:1 line.

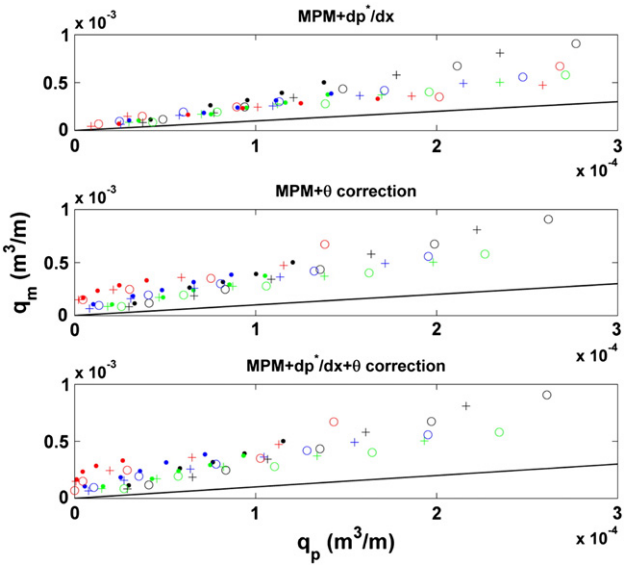

Fig. 13. Measured versus predicted transport, q_p, using MPM with dp^*/dx (top), MPM with bed slope correction (middle) and MPM with both dp^*/dx and Shields slope correction (bottom) for $D_{50} = 0.22$ mm (black), 0.5 mm (green), 0.9 mm (blue) and 2.65 mm (red) on tan $\beta = 1/10$ (.), 1/20 (+) and 1/30 (o). Solid line is 1:1 line.

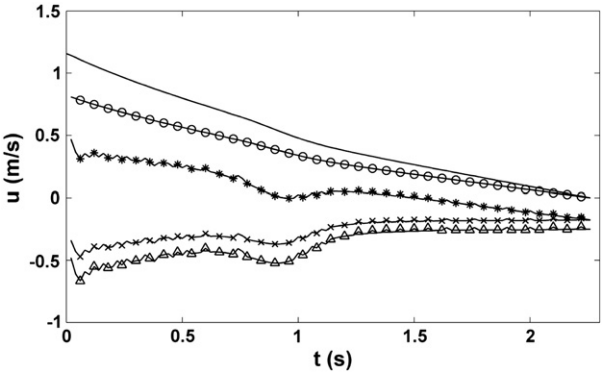

Fig. 14. Instantaneous velocity components with tan $\beta = 1/10$, $d_o = 0.24$ m and $D_{50} = 0.22$ mm. Horizontal depth averaged modelled velocity, u (•), cos $\varphi_\tau u$ (o), cos $\varphi_\tau u$ + sin $\varphi_\tau(\partial u/\partial t)/\omega$ (*), sin$\varphi_\tau(\partial u/\partial t)/\omega$ (x) and $(\partial u/\partial t)/\omega$ (Δ).

respectively. Eq. (17) has a flow depth, h, dependency and gives a time varying friction factor, $f(t)$, whilst f calculated from Eq. (12) gives a single f value for each test.

The deduced grain size dependency ranges from $p = -0.19$ to -0.65 between fine–intermediate and fine–medium sands, but $0.03 < p \leq 0.36$ between smaller and coarse grains since the coarse sand data lie above the smaller grains (Fig. 17).

4.4.7. Meyer-Peter and Muller (1948), with time varying friction via Colebrook–White and dp^*/dx

This section extends the approach of time varying friction factor to include the dp^*/dx correction, since the incorporation of dp^*/dx using a fixed f indicates an improvement in q_p for the coarse sand (Section 4.4.2). The application of the correction for dp^*/dx is similar to Section 4.4.2. On average, the total contribution from the pressure gradient reduces q_p by 3% (fine sand) to 25% (coarse sand), about the same order as the MPM + dp^*/dx model (Fig. 18). The inferred negative dependencies increase slightly between fine and larger grains excluding the coarse sand. The positive dependencies decrease for intermediate–coarse and medium–coarse sands as the gradient of the regression line for coarse sand becomes milder. The p value ranges from $p = -0.2$ to -0.72 between fine–intermediate and fine–medium sands, but $0.18 < p \leq 0.31$ between the smaller and coarse grains.

4.5. Performance of different sediment transport formulae (Brier Skill Score)

The Brier Skill Score (BSS) is commonly used in coastal engineering to assess the performance of morphological models (Van Rijn et al., 2003) and the skill score is dependent on the baseline condition. The present study adopted a similar skill score to assess the performance of each sediment transport formula, similar to the approach of van der A et al. (2010).

$$\mathrm{BSS} = 1 - \frac{\sum\left[\left(\left|q_m - q_p\right| - \Delta q_m\right)/(q_o - q_m)\right]^2}{n_d} \tag{18}$$

where n_d = number of data, Δq_m = error of measured total transport and $q_o = 0$ = baseline result. In a morphological context, the baseline condition is the initial bed level which is not zero, but for the sediment transport calculations the baseline is set to zero. The formula gives 1 for a perfect prediction, 0 for no skill, or modelling the baseline condition, and negative for prediction away from the baseline. Sutherland et al. (2004) noted that the BSS is sensitive to small changes in the value of the denominator, yielding large and unbounded negative scores when the model overpredicts.

Adoption of the BSS using Eq. (18) creates a bias if overprediction occurs. As shown in Fig. 19, if the sediment transport is overpredicted by a factor more than 2, the negative score increases rapidly compared to smaller changes in the positive score for the underprediction/overprediction by a factor less than two. For instance, consider the two scenarios of a dysfunctional transport model that underpredicts and a functional model that overpredicts. The former will give a positive score that is close to zero whilst the latter will give a large negative score. This creates a misinterpretation, in which the dysfunctional transport model always appears to be the better model. In fact, having a negative score, i.e. an overpredicting model, is better than the positive score.

Therefore, in absence of other skill scores that produce only positive numbers, Eq. (18) is used to evaluate the performance of transport models, regardless of the acknowledged drawbacks. The BSS for each model are tabulated in Table 6 and the bold values indicate the highest score or the best method of prediction. The data are best predicted via MPM followed closely by MPM + dp^*/dx. Conversely, poor predictions are obtained using other methods, particularly using Nielsen (2002) because of the use of local acceleration in the stress calculation. Overall, between a fixed f and time varying $f(t)$, the prediction using fixed f seems to give better scores. Thus in order to incorporate the grain size

Table 6
BSS of the predicted transport.

D_{50} (mm)	MPM	MPM + dp^*/dx	MPM + θ correction	MPM + dp^*/dx + θ correction	Nielsen (2002)	MPM_CW	MPM_CW + dp^*/dx
0.22	**0.58**	0.56	0.50	0.49	0.02	0.57	0.55
0.5	**0.69**	0.67	0.52	0.50	0.02	0.59	0.57
0.9	**0.67**	0.61	0.40	0.36	0.01	0.44	0.38
2.65	**0.71**	0.60	0.17	0.16	0.004	0.24	0.21

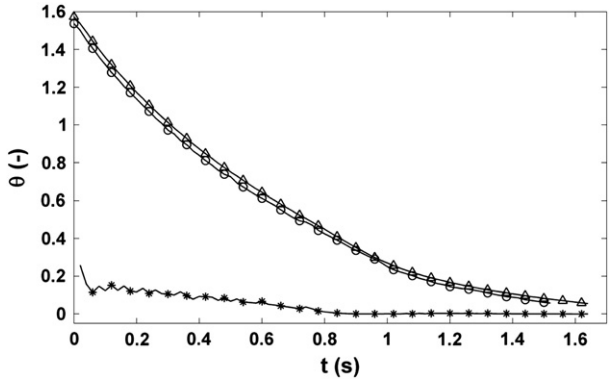

Fig. 15. Instantaneous Shields parameter, θ, with $\tan\beta = 1/10$, $d_o = 0.24$ m and $D_{50} = 0.22$ mm. $\tau/\rho(s-1)gD$ (Δ), $(\tau - \rho g\, d\eta/dx\, D)/\rho(s-1)gD$ (o) and Eq. (16) (*).

effect partly occurred through the pressure gradient, it is suggested that MPM + dp^*/dx is adopted as a general transport model for the swash zone. However, the importance of pressure gradient correction will mainly occur for large grain sizes and for larger positive pressure gradients (i.e. backwash).

4.6. p values

The overall p values deduced from the above plots are summarised in Fig. 20. Note that, in order to maintain the reliability of the p values, only data with $R^2 > 0.8$ were retained. This excludes q_p for coarse sand via Nielsen (2002). Calculations with bed slope correction are not included, as q_p versus q_m shows negligible bed slope effect in almost all the methods of prediction. The analysis for the different forcing parameters indicates:

- For a $\mathbf{U}^3$ type model: Positive q–D dependency, where q increases as D increases. The dependencies tend to have a larger positive p value between smaller–coarse grains on milder bed slopes, up to $p \approx 0.5$. This is associated with the monotonically decreasing velocity and overtopping duration as D_{50} increases.
- For the initial depth: Inverse q–D dependency, reaching $p \approx -0.9$ between fine and intermediate sands. This implicitly reflects the influence of friction on flow and hence on the transport.
- For the MPM model and variants: Inverse q–D dependency with maximum $p \approx -0.7$ between fine and intermediate sands via MPM_Colebrook–White + dp^*/dx.

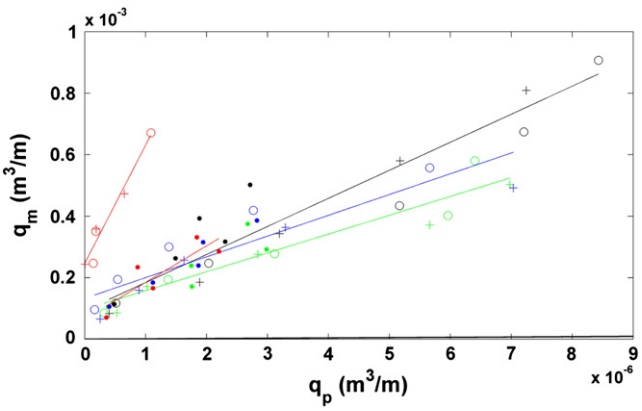

Fig. 16. Measured versus predicted transport, q_p, using Nielsen (2002) for $D_{50} = 0.22$ mm (black), 0.5 mm (green), 0.9 mm (blue) and 2.65 mm (red) on $\tan\beta = 1/10$ (.), 1/20 (+) and 1/30 (o). Solid line is 1:1 line.

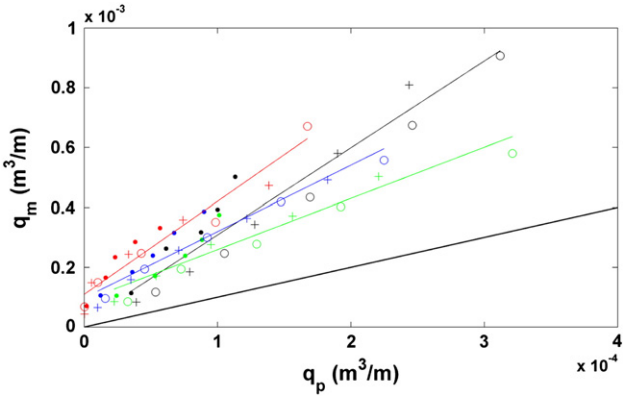

Fig. 17. Measured versus predicted transport, q_p, using MPM with time varying friction via Colebrook–White for $D_{50} = 0.22$ mm (black), 0.5 mm (green), 0.9 mm (blue) and 2.65 mm (red) on $\tan\beta = 1/10$ (.), 1/20 (+) and 1/30 (o). Solid line is 1:1 line.

Incorporation of dp^*/dx using either fixed f or time varying $f(t)$ in the uprush leads to minor increases in the negative dependency. The use of $f(t)$ over fixed f does not contribute to major differences in the deduced dependency. Overall, the average p value for different parameters is found to be narrowly ranged, around $-0.5 < p < 0.5$.

4.7. Optimum transport coefficient, C_{opt}

The optimum transport coefficients, $\mathbf{C}_{opt}$ in the MPM formulae, are calculated using the gradient of the regression lines obtained in previous section. Then, $\mathbf{C}_{opt}$ is the gradient of the regression line multiplied by the C value used in the transport calculation. This can be seen as a direct translation to obtain an optimum transport coefficient needed for a perfect prediction, i.e. $q_m = q_p$.

$$q_m = m\, q_p \tag{19}$$

$$q_p \propto F\left(C, \theta^{1.5}\right) \tag{20}$$

$$C_{opt} = mC \tag{21}$$

where m is the gradient of the regression line in q_m versus q_p plots and $C = 12$. C_{opt} values for each method of prediction are tabulated in

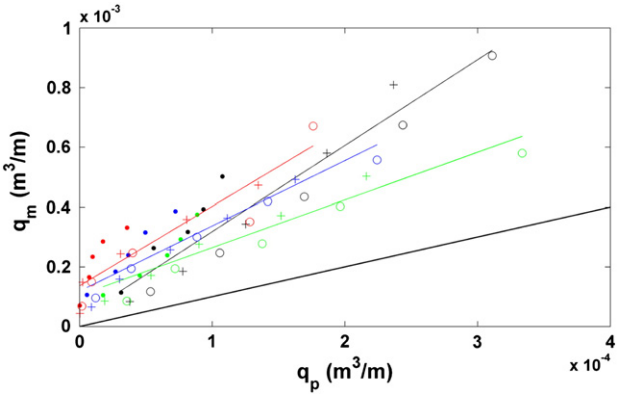

Fig. 18. Measured versus predicted transport, q_p, using MPM with time varying friction via Colebrook–White and dp^*/dx correction for $D_{50} = 0.22$ mm (black), 0.5 mm (green), 0.9 mm (blue) and 2.65 mm (red) on $\tan\beta = 1/10$ (.), 1/20 (+) and 1/30 (o). Solid line is 1:1 line.

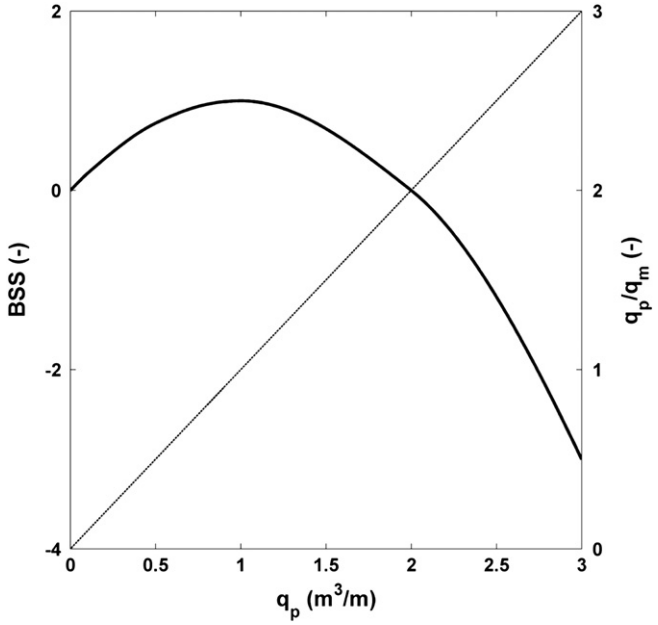

Fig. 19. Behaviour of Eq. (18) using $n = 1, q_o = 0, q_m = 1$ m^3/m and $\Delta q_m = 0$. On the left axis is BSS (-) and right axis is q_p/q_m (···).

Table 7. The bold values in Table 7 correspond to the best models from the BSS calculations in Table 6.

The average and standard deviations of the optimum transport coefficient values, $\overline{C_{opt}} \pm \sigma$, reach a maximum of 37.9 ± 3.9 for the fine sand, and vary from 23.9 ± 3.3 to 32.5 ± 8.9 for intermediate to coarse sands (Fig. 21). Small differences are obtained in C_{opt} values between grain sizes for predictions using fixed f, but the incorporation of the bed slope correction increases the discrepancy between medium and coarse sand, creating a trend of increasing C_{opt} value with increasing grain sizes. Similarly, prediction using time varying $f(t)$ also indicates larger C_{opt} values for larger grain sizes. Note that the underestimation via Nielsen (2002) yields unrealistically high C_{opt} values (of the order 100) and these are excluded from Table 6.

The findings suggest that $\overline{C_{opt}}$ is 2–3 times than the suggested value in the literature for steady flow. Further, the higher $\overline{C_{opt}}$ value is not caused by the presence of pre-suspended sediment (c.f. Masselink and Hughes, 1998), since the present study specifically and purposely excludes pre-suspended sediment. It is plausible to obtain a larger $\overline{C_{opt}}$ value for fine sand, considering the mobility and sensitivity of fine sand to pickup and suspension in comparison to the larger sands, although theoretically this should be accounted for in the Shields parameter. Nevertheless, there is no apparent trend of $\overline{C_{opt}}$ values for other sand sizes.

The results of the deduced transport–grain size relationships are not changed even if the velocity is not perfectly modelled. This is because a constant increase/decrease in the predicted velocity would change the slope of the regression line by the same amount but the ratio of these slopes and the grain size dependency remain the same as per Eq. (1). The only influence of the predicted velocity is on the inferred sediment transport coefficients, which will be lower if the model over predicts and vice versa.

5. Conclusion

New sediment transport experiments have investigated the influence of grain size and pressure gradients on unsteady sediment transport, with

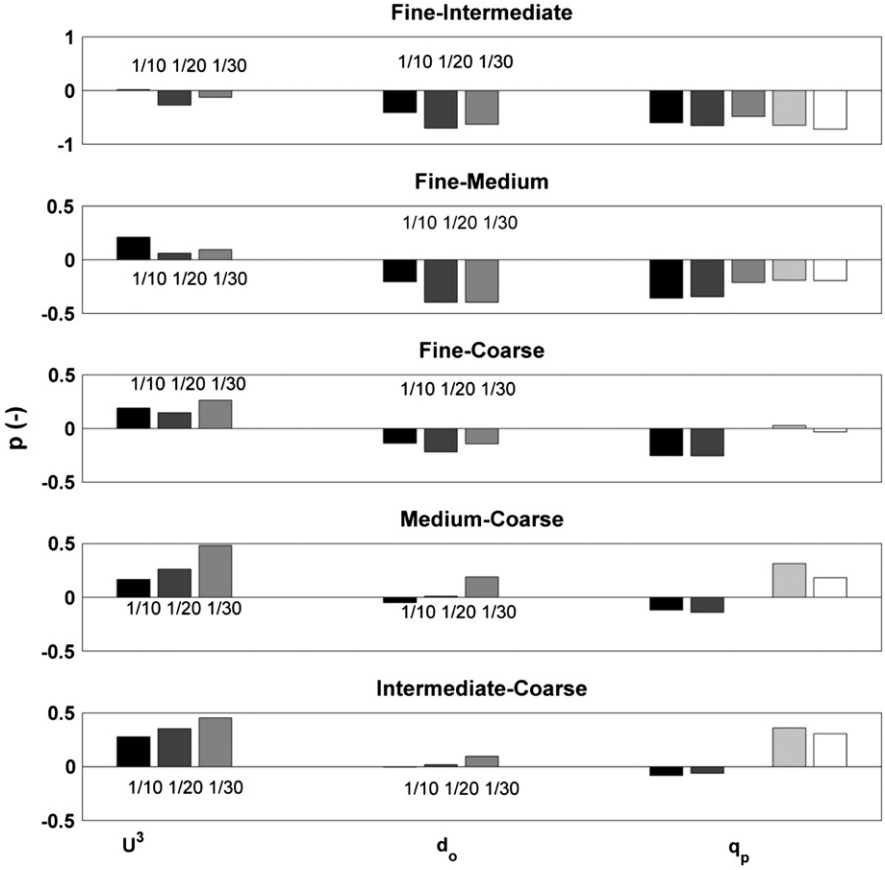

Fig. 20. p values for different forcing parameters. For q_p, bars show results for different variations of the MPM model. MPM (■), MPM + dp^*/dx (▬), Nielsen (▬), MPM_CW (▭) and MPM_CW + dp^*/dx (□).

Table 7
C_{opt} values using calculated θ_{cr}.

D_{50}(mm)	MPM	MPM + dp^*/dx	MPM + θ correction	MPM + dp^*/dx+θ correction	Nielsen (2002)	MPM_CW	MPM_CW + dp^*/dx
0.22	**41.8**	41.8	42.7	42.6	1095.1	34.9	34.5
0.5	**25.5**	24.4	27.4	26.2	735.1	20.5	19.1
0.9	**25.2**	25.7	29.8	29.7	810.7	26.6	26.2
2.65	**22.2**	22.1	43.6	38.0	1087.9	37.3	31.9

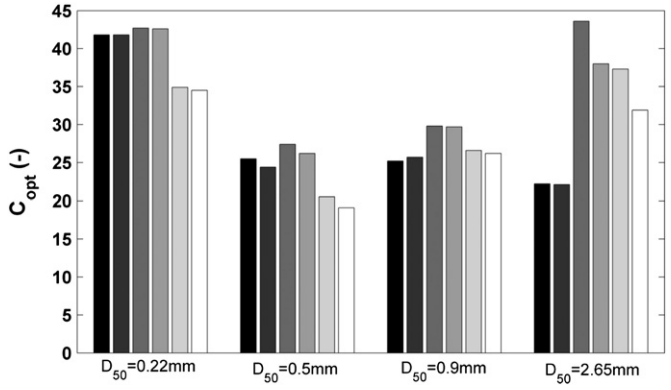

Fig. 21. C_{opt} values for different variations of the MPM model. MPM (■), MPM + dp^*/dx (■), MPM + θ correction (▬), MPM + dp^*/dx + θ correction (▬), MPM_CW (▭) and MPM_CW + dp^*/dx (□).

application to swash zone flows. Assuming a relationship of the form $q \propto D^p$, the $q - D$ dependencies are deduced for a range of flow parameters. These include the initial dam depth, d_o, the time integrated predicted depth averaged velocity cubed, $\boldsymbol{U}^3 = \int u^3 dt$, and the predicted transport, q_p, using the Meyer-Peter and Muller (1948) transport model and a number of variants to that model. The data shows different dependencies are obtained depending on the chosen parameters. Overall, negative dependencies ($p < 0$) are obtained for d_o and q_p whilst positive dependencies ($p > 0$) are obtained for $\boldsymbol{U}^3$. The p value is found to be narrow ranged, $0.5 < p < -0.5$. The negative dependency of $p \approx -0.5$ is consistent with Bagnold's (1980, 1986) but contradicts the Meyer-Peter Muller model, which theoretically has $p \approx 1$. Despite this, the MPM model provides the most consistent estimates of the transport, i.e. the best correlation coefficients.

Incorporation of a pressure gradient correction in the transport calculation moderately improved the transport predictions for larger grains sizes. On average, the total contribution of the pressure gradient reduces the total transport prediction by 3% (fine sand) to 18% (coarse sand). It is suggested that future general swash sediment transport models should incorporate the grain size effect, partly through the pressure gradient. However, the importance of this correction will mainly occur for large grain sizes and for larger positive pressure gradients, i.e. in the backwash.

Overall, the derived dependencies based on q_p are not affected by the prediction using either fixed or time varying friction factor. Moreover, the measured and predicted transport potential over sloping beds does not show a significant bed slope effect, at least for the velocities tested herein. Using the Brier Skill Score, the data are best predicted via MPM followed closely by MPM + dp^*/dx. It is found that the average optimum transport coefficient obtained for the data is significantly larger than the suggested in the literature, $\overline{C_{opt}} \approx 30$ and this is not caused by the presence of the pre-suspended sediment. The value of the optimum transport coefficient is larger for fine grains but there is no apparent trend for other sand sizes.

Acknowledgements

The first author is indebted to the Ministry of Higher Education of Malaysia and the Universiti Teknologi Malaysia for providing scholarship and financial support.

References

Bagnold, R.A., 1956. The flow of cohesionless grains in fluids. Proc. R. Soc. Lond. A 249 (964), 235–297.
Bagnold, R.A., 1980. An empirical correlation of bedload transport rates in flumes and natural rivers. Proc. R. Soc. Lond. A 372 (1751), 453–473.
Bagnold, R.A., 1986. Transport of solids by natural water flow: evidence for a worldwide correlation. Proc. R. Soc. Lond. A 405 (1829), 369–374.
Bailard, J.A., Inman, D.L., 1981. An energetics bedload model for a plane sloping beach: local transport. J. Geophys. Res. 86 (C3), 2035–2043.
Baldock, T.E., 2012. Discussion of "Laboratory investigation of pressure gradients induced by plunging breakers", by Pedrozo-Acuña et al Coast. Eng. 66, 1–2.
Baldock, T.E., Hughes, M.G., 2006. Field observations of instantaneous water slopes and horizontal pressure gradients in the swash-zone. Cont. Shelf Res. 26 (5), 574–588.
Baldock, T.E., Nielsen, P., 2010. Discussion of "Effect of seepage-induced nonhydrostatic pressure distribution on bed-load transport and bed morphodynamics" by Simona Francalanci, Gary Parker, and Luca Solari. J. Hydraul. Eng. 136 (1), 77–79.
Baldock, T., Hughes, M., Day, K., Louys, J., 2005. Swash overtopping and sediment overwash on a truncated beach. Coast. Eng. 52 (7), 633–645.
Barnes, M.P., 2009. Measurement and modelling of swash zone bed shear stress. (PhD Thesis) University of Queensland.
Barnes, M.P., Baldock, T.E., 2010. A lagrangian model for boundary layer growth and bed shear stress in the swash zone. Coast. Eng. 57 (4), 385–396.
Briganti, R., Dodd, N., Kelly, D., Pokrajac, D., 2012. An efficient and flexible solver for the simulation of the morphodynamics of fast evolving flows on coarse sediment beaches. Int. J. Numer. Methods Fluids 69 (4), 859–877.
Del Valle, R., Medina, R., Losada, M., 1993. Dependence of coefficient k on grain size. J. Waterw. Port Coast. Ocean Eng. 119, 568.
Dohmen-Janssen, C.M., 1999. Grain size influence on sediment transport in oscillatory sheet flow: phase lags and mobile-bed effects. (PhD Thesis) Delft University of Technology.
Dohmen-Janssen, C.M., Hanes, D.M., 2002. Sheet flow dynamics under monochromatic nonbreaking waves. J. Geophys. Res. 107 (10.1029).
Dohmen-Janssen, C.M., Hassan, W.N., Ribberink, J.S., 2001. Mobile-bed effects in oscillatory sheet flow. J. Geophys. Res. 106 (C11), 27,103–27,115.
Flores, N.Z., Sleath, J.F.A., 1998. Mobile layer in oscillatory sheet flow. J. Geophys. Res. 103 (C6), 12783–12793.
Fredsoe, J., Deigaard, R., 1992. Mechanics of Coastal Sediment Transport. World Scientific, Singapore (369 pp.).
Hassan, W.N.M., Ribberink, J.S., 2010. Modelling of sand transport under wave-generated sheet flows with a rans diffusion model. Coast. Eng. 57 (1), 19–29.
Hogg, A.J., Baldock, T.E., Pritchard, D., 2011. Overtopping a truncated planar beach. J. Fluid Mech. 666, 521–553.
Hughes, M.G., Masselink, G., Brander, R.W., 1997. Flow velocity and sediment transport in the swash zone of a steep beach. Mar. Geol. 138 (1–2), 91–103.
Kelly, D.M., Dodd, N., 2010. Beach-face evolution in the swash zone. J. Fluid Mech. 661 (12), 316–340.
Khezri, N., Chanson, H., 2012. Undular and breaking bores on fixed and movable gravel beds. J. Hydraul. Res. 50 (4), 353–363.
King, D., 2005. Influence of grain size on sediment transport rates with emphasis on the total longshore rate. Coastal Hydraulics Lab Development Center Vicksburg, ERDC/CHL CHETN-II-48.
Kranenburg, W.M., Ribberink, J.S., Schretlen, J.J.L.M., Uittenbogaard, R.E., 2013. Sand transport beneath waves: the role of progressive wave streaming and other free surface effects. J. Geophys. Res. Earth Surf. 118 (1), 122–139.
Martin, Y., Church, M., 2000. Re-examination of Bagnold's empirical bedload formulae. Earth Surf. Process. Landforms 25 (9), 1011–1024.
Masselink, G., Hughes, M., 1998. Field investigation of sediment transport in the swash zone. Cont. Shelf Res. 18 (10), 1179–1199.
Masselink, G., Russell, P., Blenkinsopp, C., Turner, I., 2010. Swash zone sediment transport, step dynamics and morphological response on a gravel beach. Mar. Geol. 274 (1–4), 50–68.
Meyer-Peter, E., Muller, R., 1948. Formulas for bed-load transport. Proceedings 2nd International IAHR Congress, Stockholm, Sweden, pp. 39–64.
Microsonic, 2010. mic + 25/DD/TC/E. http://www.microsonic.de/en/Products/micplus/SPECIAL-EQUIPMENT/mic25DDTCE.htm.
Néelz, S., Pender, G., 2010. Benchmarking of 2d Hydraulic Modelling Packages. Environment Agency, Bristol, UK.
Nielsen, P., 1992. Coastal Bottom Boundary Layers and Sediment Transport. World Scientific Pub Co Inc.
Nielsen, P., 2002. Shear stress and sediment transport calculations for swash zone modelling. Coast. Eng. 45 (1), 53–60.
Nielsen, P., 2006. Sheet flow sediment transport under waves with acceleration skewness and boundary layer streaming. Coast. Eng. 53 (9), 749–758.

Nielsen, P., Callaghan, D.P., 2003. Shear stress and sediment transport calculations for sheet flow under waves. Coast. Eng. 47 (3), 347–354.
O'Donoghue, T., Wright, S., 2004. Flow tunnel measurements of velocities and sand flux in oscillatory sheet flow for well-sorted and graded sands. Coast. Eng. 51 (11–12), 1163–1184.
Pedrozo-Acuña, A., de Alegría-Arzaburu, A.R., Torres-Freyermuth, A., Mendoza, E., Silva, R., 2011. Laboratory investigation of pressure gradients induced by plunging breakers. Coast. Eng. 58 (8), 722–738.
Postacchini, M., Brocchini, M., Mancinelli, A., Landon, M., 2012. A multi-purpose, intra-wave, shallow water hydro-morphodynamic solver. Adv. Water Resour. 38, 13–26.
Puleo, J.A., Beach, R.A., Holman, R.A., Allen, J.S., 2000. Swash zone sediment suspension and transport and the importance of bore-generated turbulence. J. Geophys. Res. 105 (C7), 17021–17044.
Puleo, J.A., Holland, K.T., Plant, N.G., Slinn, D.N., Hanes, D.M., 2003. Fluid acceleration effects on suspended sediment transport in the swash zone. J. Geophys. Res. 108 (C11), 3350.
Puleo, J.A., Farhadzadeh, A., Kobayashi, N., 2007. Numerical simulation of swash zone fluid accelerations. J. Geophys. Res. 112 (C7), C07007.
Schretlen, J.L.M., Ribberink, Jan S., O'Donoghue, T., 2011. Boundary layer flow and sand transport under full scale surface waves. Proceedings of 32nd Conference on Coastal Engineering. Shanghai, China, pp. 1–14.
Shields, A., 1936. Application of similarity principles and turbulence research to bed-load movement.
Sleath, J.F.A., 1984. Sea Bed Mechanics. John Wiley & Sons, New York.
Sumer, B.M., Kozakiewicz, A., Fredsoe, J., Deigaard, R., 1996. Velocity and concentration profiles in sheet-flow layer of movable bed. J. Hydraul. Eng. 122 (10), 549–558.
Sutherland, J., Peet, A.H., Soulsby, R.L., 2004. Evaluating the performance of morphological models. Coast. Eng. 51 (8–9), 917–939.
Swamee, P.K., Jain, A.K., 1976. Explicit equations for pipe-flow problems. J. Hydraul. Div. 102 (5), 657–664.
Teakle, I.A.L., 2006. Coastal boundary layer and sediment transport modelling. (PhD Thesis) University of Queensland.
van der A, D.A., O'Donoghue, T., Ribberink, J.S., 2010. Measurements of sheet flow transport in acceleration-skewed oscillatory flow and comparison with practical formulations. Coast. Eng. 57 (3), 331–342.
Van Rijn, L., 1993. Principles of Sediment Transport in Rivers, Estuaries, and Coastal Seas. Aqua publications.
Van Rijn, L., et al., 2003. The predictability of cross-shore bed evolution of sandy beaches at the time scale of storms and seasons using process-based profile models. Coast. Eng. 47 (3), 295–327.
van Rijn, L.C., Walstra, D.J.R., van Ormondt, M., 2007. Unified view of sediment transport by currents and waves. IV: Application of morphodynamic model. J. Hydraul. Eng. 133 (7), 776.
Van Wellen, E., Chadwick, A.J., Mason, T., 2000. A review and assessment of longshore sediment transport equations for coarse-grained beaches. Coast. Eng. 40, 243–275.
Watanabe, A., Sato, S., 2004. A sheet-flow transport rate formula for asymmetric forward-leaning waves and currents. Proceedings of the 29th Conference on Coastal Engineering, pp. 1703–1714.
Young, Y., Xiao, H., Maddux, T., 2010. Hydro-and morpho-dynamic modeling of breaking solitary waves over a fine sand beach. Part I: experimental study. Mar. Geol. 107–118.